ADVANCED MATERIALS INTERFACES
www.advmatinterfaces.de

Selectivity Enhancement for Ruthenium Atomic Layer Deposition in Sub-50 nm Nanopatterns by Diffusion and Size-Dependent Reactivity

*Jan-Willem J. Clerix, Esteban A. Marques, Job Soethoudt, Fabio Grillo, Geoffrey Pourtois, J. Ruud Van Ommen, and Annelies Delabie**

Area-selective deposition (ASD) is a promising bottom-up approach for fabricating nanoelectronic devices. However, a challenge is to prevent the undesired growth of nanoparticles in the nongrowth area. This work uses kinetic Monte Carlo (KMC) methods to investigate the defectivity in ruthenium ASD by (ethylbenzyl)(1-ethyl-1,4-cyclohexadienyl)Ru/O_2 (EBECHRu) atomic layer deposition (ALD) in line-space nanopatterns with different dimensions. Ru ASD is governed by adsorption as well as diffusion. The defectivity depends on the pattern dimensions, as nanoparticles can diffuse and reach the interface with the growth area where they aggregate. For linewidths of 50 nm and smaller, all Ru adspecies are captured at the growth interface before growth by precursor adsorption is catalyzed. The synergetic effect of diffusion and size-dependent reactivity reduces defectivity below 10^{10} Ru atoms cm^{-2} for at least 1000 ALD cycles. This is more than 1000 times lower than for patterns with a linewidth of 200 nm and larger, where the Ru content decreases significantly only near the interface with the growth surface. The predicted depletion zone is confirmed by experiments in nanoscale line-space patterns. Overall, this mechanism results in smaller and fewer Ru nanoparticles for smaller patterns, facilitating the development of passivation-deposition-etch ASD processes for nanoelectronic device fabrication.

1. Introduction

The semiconductor industry continuously improves the performance and power consumption of nanoelectronic devices by decreasing device dimensions, by implementing new materials and by introducing new device concepts and architectures. As a consequence, the device fabrication processes by classic top-down lithography and patterning are becoming increasingly complex and expensive.[1] Area-selective deposition (ASD) promises to simplify and improve the fabrication processes.[2,3] ASD aims to grow materials only where needed, from the bottom up, by selective deposition on one surface area, the growth surface, while preventing growth on another area, the nongrowth surface. As such, nanopatterns can be replicated or small features can be filled up from the bottom. ASD can simplify and improve the fabrication process by reducing the number of steps, limit edge placement errors, and offer a new patterning paradigm.[4,5]

The selectivity of chemical vapor deposition (CVD) processes is known to rely on different kinetics of the adsorption, desorption, and diffusion processes on the growth and nongrowth surface area.[6] Fast adsorption and fast reactions on the growth surface lead to film growth. Selective deposition occurs when adsorption on the nongrowth surface is much slower, by fluxes of intermediate species from the nongrowth to growth area by surface and/or gas phase diffusion, and/or by etch and desorption processes of intermediate species on the nongrowth surface. These kinetics in selective epitaxy by high-temperature CVD are often process inherent but can be improved by surface modification.[7–9] The roles of gas phase and surface diffusion have long been known in selective epitaxial growth by CVD.[6,7,10–20] The resulting fluxes reduce deposition on the nongrowth surface and enhance the growth rate on the growth surface. As a consequence, the growth rate and selectivity depend on the pattern dimensions and geometry when the pattern dimensions are comparable or smaller than the characteristic diffusion length.[6,12,21–23] For example, diffusion processes in selective Si epitaxy by $SiCl_4/H_2$ CVD at 1200 °C are characterized by diffusion lengths

J. J. Clerix, E. A. Marques, J. Soethoudt, A. Delabie
Department of Chemistry
KU Leuven
Celestijnenlaan 200F, Heverlee 3001, Belgium
E-mail: Annelies.Delabie@imec.be
J. J. Clerix, E. A. Marques, J. Soethoudt, A. Delabie, G. Pourtois
Imec
Kapeldreef 75, Heverlee 3001, Belgium
F. Grillo
Department of Materials
ETH Zurich
Zurich 8093, Switzerland
J. R. Van Ommen
Department of Chemical Engineering
TU Delft
Delft 2629 HZ, The Netherlands

The ORCID identification number(s) for the author(s) of this article can be found under https://doi.org/10.1002/admi.202100846.

DOI: 10.1002/admi.202100846

in the µm range, at least partially driven by the very high temperatures of these processes.[6,24] The impact of surface diffusion and aggregation was recently also demonstrated for Ru ASD by (carbonyl)(cyclohexadienyl)Ru/H_2 CVD at a much lower deposition temperature of 250 °C, driven by high surface energy of Ru and the low surface energy of the methyl-terminated SiO_2 nongrowth surface.[12] The experimental-theoretical study indicated an average diffusion length of 140 nm for Ru adspecies on the methyl-terminated SiO_2 nongrowth substrate. Indeed, diffusion-mediated Ru ASD was observed in SiO_2-TiN line-space patterns with a critical dimension of 45 nm and SiO_2 line height of 60 nm. Depletion of Ru nanoparticles near the interface with the growth surface and a more than two times higher growth rate for ASD compared to CVD is consistent with diffusion of Ru adspecies from the nongrowth to the growth area, where they contribute to Ru growth.[12,25] Almost no Ru deposition was present on the SiO_2 sidewalls, indicating that diffusion can be an ally in defect mitigation.

While the concept of diffusion-mediated ASD is widely described for high-temperature CVD, only a few papers discuss the role of diffusion in area-selective atomic layer deposition (AS-ALD) in nanopatterns at moderate temperatures.[13,14,26] The selectivity of AS-ALD has so far mostly been established by tuning the adsorption and desorption processes, for example by using organic blocking layers, self-assembled monolayers, small inhibitor molecules, and/or by etching the nanoparticles that can grow on the nongrowth area.[3,27] Interestingly, few studies of diffusion processes during ALD exist. For example, diffusion and aggregation processes have been proposed for trimethyl(methylcyclopentadienyl)Pt/O_2 ALD of Pt nanoparticles on SiO_2 and graphene and for (ethylbenzyl)(1-ethyl-1,4-cyclohexadienyl)Ru/O_2 (EBECHRu) ALD of Ru nanoparticles on organosilicate glass (OSG).[13,28–31] While the role of diffusion is known, the impact on selectivity is not observed yet. This could be related to the lack of studies in patterns with nanoscale dimensions: high impact on selectivity is expected especially in patterns with dimensions in the same order of magnitude as the diffusion length, which is only 16 nm for Ru adspecies in the EBECHRu/O_2 Ru ALD process on OSG.[13,19,32] Another interesting feature of this Ru ALD process is the size-dependent reactivity of Ru nanoparticles. Ru nanoparticles that are too small to catalyze O_2 dissociation do not grow by precursor adsorption, which intrinsically limits the nanoparticle growth. This phenomenon is highly interesting in view of selectivity. However, this Ru AS-ALD process has not been studied extensively in patterns with nanoscale dimensions, where diffusion and size-dependent reactivity may affect selectivity. In addition, these dimensions are highly relevant for ASD applications in nanoelectronic device fabrication, where insight into the ASD mechanism, the defect density, and defect sizes is important for the design of defect mitigation strategies (such as periodic passivation and etching).[2,3,33–37]

Therefore, in this paper, we investigate the mechanism of Ru ASD to understand the impact of adsorption and diffusion on defectivity and selectivity in nanoscale line patterns with line widths between 20 and 200 nm. We quantify the density and size of Ru nanoparticles on an area-restricted non-growth surface as a function of the line width through simulations. The theoretical predictions are supported by experimental results for Ru ASD in nanoscale patterns.

2. Results and Discussion

2.1. Ru ALD Growth Mechanism on Blanket Substrates

In order to study patterned SiO_2 surfaces through simulations, the growth mechanism on blanket (nonpatterned) surfaces should first be described. The growth mechanism of EBECHRu/O_2 ALD on a blanket OSG was already determined in a previous study.[13] However, the pristine OSG surface is not representative for ASD as the surface composition changes from methyl-terminated OSG to hydroxyl-terminated SiO_2 during the patterning processes, and restoration of the methyl-termination is required to enable Ru ASD by ALD, for example by *N,N*-dimethylamino-trimethylsilane (DMA-TMS).[32,38,39] We therefore first investigate the Ru ALD growth mechanism on blanket SiO_2 substrates passivated with DMA-TMS (SiO_2-$OSi(CH_3)_3$). SiO_2 is an omnipresent material in nanoelectronics and is a typical nongrowth surface for many practical implementations of Ru ASD. Passivation of SiO_2 by DMA-TMS is known to reduce precursor adsorption in many ALD processes.[32,39,40] DMA-TMS exposure is compatible with back-end-of-line processing. In this study, we therefore determine the simulation parameters of EBECHRu/O_2 ALD on the blanket SiO_2-$OSi(CH_3)_3$ substrates, based on previously published experimental growth curves.[32] These experiments were conducted in identical experimental conditions as the preceding study on OSG by our group, so that the impact of the surface can be investigated.[13] The growth curves are compared in Figure 2 and the experimental conditions are included in the Experimental section for reference.

The fundamental processes in the kinetic Monte Carlo (KMC) model used to simulate Ru ALD have been previously described by Soethoudt et al.[13] KMC methods allow simulation of the most important processes in Ru ALD in the relevant spatial (100's of nanometers) and temporal (multiple cycles) frames. The microscopic evolution of the system is determined by a limited set of events with known probability. The model describes the evolution of the particle size distribution (PSD, see Supplementary Information), the total amount of Ru (Ru atom areal density), nanoparticle number density, and surface coverage during EBECHRu/O_2 ALD on dielectric substrates.[32,41] We define the most important quantities for ALD on non-growth surfaces as follows:

- The PSD is the normalized probability of finding a Ru nanoparticle of a given radius on the nongrowth area.
- The Ru atom areal density is the amount of Ru atoms per unit surface area (at cm^{-2}) of the nongrowth surface area.
- The Ru nanoparticle number density is the amount of Ru nanoparticles per unit surface area (cm^{-2}) of the nongrowth surface area.
- The coverage is the percentage of the non-growth area covered by Ru nanoparticles.
- The growth-per-cycle (GPC) is the amount of Ru atoms deposited per unit area and cycle (at cm^{-2} cy^{-1}) on the nongrowth area.
- The steady-state GPC is the growth rate of Ru ALD on a blanket Ru substrate or on the surface of a Ru nanoparticle (nm cy^{-1}).

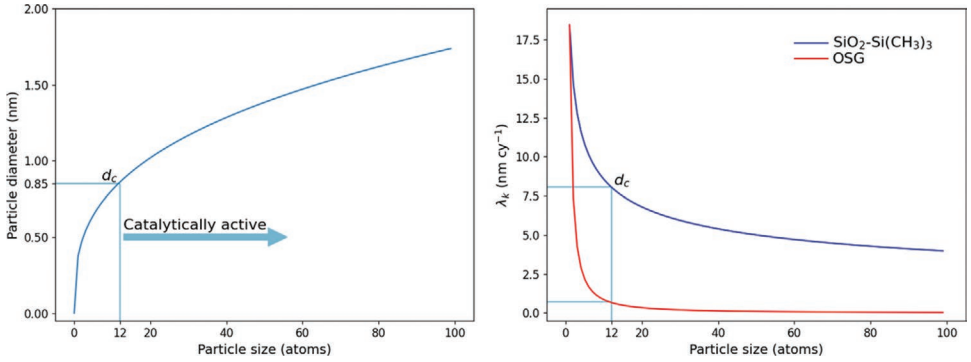

Figure 1. Left: particle diameter (nm) as a function of particle size (atoms). Particles of at least 12 atoms have reached d_c and are catalytically active toward O_2 dissociation, i.e., they will also grow through fast precursor adsorption on the particle itself. Right: λ_k (nm cy^{-1}) as a function of particle size (atoms). At size 1, λ_k is the average diffusion length of an adatom. For a Ru adatom on SiO_2-OSi(CH$_3$)$_3$ this is 18 nm cy^{-1} as determined in this study, on OSG, this is 16 nm cy^{-1} as determined previously.[13] The λ_k of Ru particles on SiO_2-OSi(CH$_3$)$_3$ is halved by the time they reach the critical diameter (d_c); after which it reduces continuously at a slower rate. On OSG, the size-dependence of λ_k is much more pronounced and particles at $d_c$are effectively immobile.

The simulated substrate is a 2D lattice with square sites with sides of 0.356 nm, the diameter of a Ru atom. Ru adatoms are deposited on the uncovered part (i.e., not covered by Ru particles) of the starting SiO_2-OSi(CH$_3$)$_3$ surface each cycle, parametrized as G_s (at nm^{-2}). G_s was experimentally determined as the Ru atom areal density after 1 ALD cycle through total X-ray fluorescence spectroscopy (TXRF), i.e., it is the GPC in the first Ru ALD cycle. 6.3×10^{-4} at nm^{-2} are instantaneously deposited on the free surface at the start of every simulated cycle in a random spatial distribution.

On this surface, Ru adspecies are able to diffuse as described by the power law (Equation 1):

$$D_k = D_1\, k^{-s} \tag{1}$$

where D_k is the average diffusion coefficient of a particle of k atoms (nm^2 cy^{-1}), D_1 is the average diffusion coefficient of a Ru adatom (nm^2 cy^{-1}) and s (-) is a factor that describes the decrease in diffusion length with particle size. The adatoms and particles diffuse over the surface and irreversibly aggregate with each other to form new hemispherical particles composed of the combined number of atoms. An average diffusion length (nm cy^{-1}) of a particle of k atoms can be defined as (Equation 2, **Figure 1**, right):

$$\lambda_k = \sqrt{D_k} \tag{2}$$

D_1 and s were determined by fitting the experimental PSD, Ru atom areal density, nanoparticle number density, and coverage through a previously published mean-field model to experimental data.[13,28] The determined parameters correspond to Ru ALD at 325 °C with a 5s EBECHRu, 5s N_2, 0.4s O_2, 3s N_2 cycle (see Experimental section). The diffusion parameters of a similar Pt ALD process were shown to depend on O_2-coreagent pulse length and substrate temperature; however, these parameters are not investigated here.[11]

Collisions of Ru adatoms and/or nanoparticles lead to instantaneous, irreversible aggregation due to the limited temperature (325 °C) and high pair bond energy, also seen in the irreversible integration of Ru nanoparticles in Ru films at the interface with the growth area.[12,42,43] The Ru nanoparticles are hemispherical, with a height to radius ratio of 1, which was determined by transmission electron microscopy (TEM, Supporting Information). The surface area is approximated as an hcp-truncated hexagonal bipyramid [1011]+[0001].[44,45]

Diffusion of adatoms and nanoparticles on blanket substrates is described accurately by applying periodic boundary conditions.[13] Species that diffuse across one of the sides of the 700 nm by 700 nm simulated substrate reappear on the opposite side. The simulations were repeated until a total 10^7 nm^2 substrate area was simulated.

Only when a particle has grown through diffusion and aggregation to reach a critical diameter (d_c) of 0.85 nm, it becomes catalytically active toward O_2 dissociation.[13,46] This diameter corresponds to particles of at least 12 atoms (Figure 1, left). The catalytic activity allows the direct adsorption of Ru precursors on the Ru particle each cycle, which results in a constant radial growth of 0.03 nm cy^{-1}, as determined to be the steady-state GPC of Ru ALD on a Ru surface in refs. [13,41] To obtain a constant radial growth, the number of deposited atoms depends on the surface area of the hemispherical hcp-truncated hexagonal bipyramid [1011]+[0001] particle and is determined by the parameter G_p (at (surf. at)$^{-1}$). Therefore, 0.1261 Ru atoms are deposited per surface atom of the nanoparticle (>d_c). Direct deposition on the particle is characteristic of the Ru material and ALD process conditions and is independent of the dielectric substrate type. In the simulations, particles grow instantaneously at the start of each cycle.

The parameters that describe Ru ALD on SiO_2-OSi(CH$_3$)$_3$ are compared to those of OSG in **Table 1**. Overall, we observe a less pronounced growth inhibition on SiO_2-OSi(CH$_3$)$_3$ than on OSG in the experimental growth curves (**Figure 2**). TXRF shows a slightly higher deposition rate on the surface (G_s) on SiO_2-OSi(CH$_3$)$_3$ than on OSG. One possible cause for the higher deposition rate is the higher −OH group density on SiO_3-OSi(CH)$_3$ (0.4 nm^{-2}) compared to OSG (<0.1 nm^{-1}).[10,24] The critical diameter (for catalysis of O_2 dissociation) and the deposition rate on the Ru particles are independent of the substrate.

The different growth behavior of Ru ALD on the two substrates is also attributed to differences in the diffusion kinetics.

Table 1. Parameters for KMC simulations of Ru ALD on the OSG and SiO_2-$OSi(CH_3)_3$ surfaces.

	OSG	SiO_2-$OSi(CH_3)_3$
Gs	1.5 10^{-4} at nm^{-2} cy^{-1}	6.3 10^{-4} at nm^{-2} cy^{-1}
D_1	270 nm^2 cy^{-1}	340 nm^2 cy^{-1}
s	8/3	2/3
Gp	0.1261 at (surf. at.)$^{-1}$ cy^{-1}	
dc	0.85 m	

Adatom diffusion is slightly faster on the SiO_2-$OSi(CH_3)_3$ surface (D_1), and particle diffusion is less size-dependent (s) than on OSG. A size dependence s <1 on SiO_2-$OSi(CH_3)_3$ indicates that even large particles will continue to be mobile. Especially for particles larger than d_c, λ_k reduces slower with particle size (Figure 1, right). On OSG, diffusion and aggregation will only be of importance for adatoms and small clusters (<d_c). On SiO_2-$OSi(CH_3)_3$, the greater mobility will result in the formation of larger particles than on OSG. At the same time, the larger diffusion lengths of adatoms and nanoparticles will reduce the nanoparticle number density. The larger diffusion lengths on SiO_2-$OSi(CH_3)_3$ might be attributed to differences in surface composition and roughness. The surface roughness of SiO_2-$OSi(CH_3)_3$ (RMS = 0.14 nm) is lower compared to OSG (0.79 nm), as determined by AFM (see Supporting Information).

2.2. Ru ASD Growth Mechanism on 200 nm Wide Line Patterns: Model and Experiment

Ru ALD on SiO_2-$OSi(CH_3)_3$ nanopatterns is expected to behave differently than Ru ALD on nonpatterned substrates, as the surface diffusion and aggregation near the growth/nongrowth interface can affect the growth rate, density, and spatial distribution of Ru nanoparticles. In the next step, we therefore simulate the growth behavior in area restricted nongrowth surfaces.

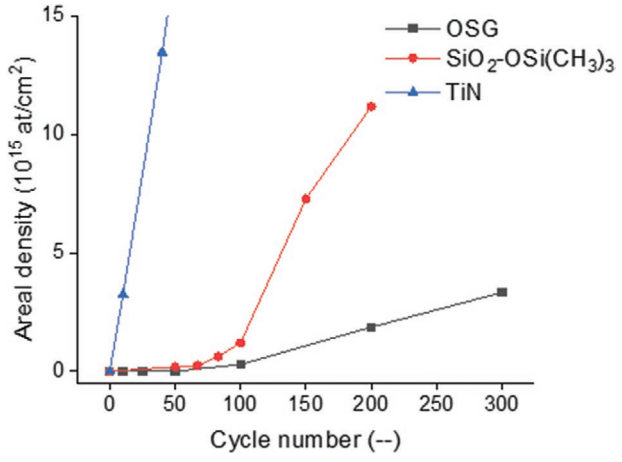

Figure 2. Experimental growth curves of Ru ALD at 325 °C on OSG, SiO_2-$OSi(CH_3)_3$, and TiN. Growth curve on SiO_2-$OSi(CH_3)_3$ obtained as discussed in the Experimental section. Growth curves on OSG and TiN taken from ref. [13,38].

These serve to approximate the experimental line-space patterns as described later in this paper (**Figure 3**). The existing KMC code was therefore modified to describe deposition on the area restricted nongrowth area of heterogeneous substrates. Nanoparticle growth on the nongrowth surface is described in the same manner as for Ru ALD on the SiO_2-$OSi(CH_3)_3$ blanket substrates. In this approximation, we therefore neglect the impact of minor changes in surface composition that may occur due to the patterning processes. However, the impact of left and right interfaces with a growth surface area is assumed to act as particle sinks: particles that reach the interfaces are removed from the simulation to mimic irreversible aggregation and incorporation into the growing Ru film on the growth surface (Figure 3). This has been shown to be an appropriate assumption in other diffusion-mediated Ru ASD processes.[12] Periodic boundary conditions are applied along the depth direction. The linear Ru ALD growth on the growth surface is not modeled explicitly. As such we model the impact of the restricted surface area of the non-growth area and the proximity of interfaces with the growth area. As the hypothetical Ru film is not explicitly incorporated, the possible overgrowth of Ru onto the nongrowth surface is not considered in the simulations. This is in keeping with the application of ASD in a line-space pattern, where lateral overgrowth is not a concern. Note that in planar line patterns lateral overgrowth might be possible and might be enhanced by diffusion from the non-growth area.

Area-restricted substrates with widths between 20 and 200 nm were simulated, to investigate the impact of the line width on the ASD mechanism. For the 200 nm wide area-restricted substrate, the line width is an order of magnitude larger than the average diffusion length of a Ru adatom (18 nm). The depth of the substrate unit cell was fixed at 700 nm. For each area-restricted substrate, a total substrate area of over 10^7 nm^2 was simulated. These surfaces were exposed to up to 167 cycles of Ru ALD. However, we will focus mainly on the range 50–100 cycles, as this corresponds to the thicknesses (2.5–5 nm) of interest for possible ASD applications of the Ru ALD process.[38] For the smallest area-restricted substrates with widths of 20 and 50 nm, up to 1000 cycles were simulated. The results of these simulations for 200 nm wide area-restricted substrate are compared to those for blankets in **Figure 4**.

As predicted, the Ru surface coverage, Ru atom areal density, and nanoparticle number density for Ru ALD on the 200 nm area-restricted substrate are lower as compared to Ru ALD on blanket substrates. The Ru nanoparticle number density is 35% lower on the area-restricted substrate after 50 ALD cycles. The decreased surface coverage and Ru atom areal density are a result of the reduced Ru nanoparticle number density. The Ru nanoparticle number density decreases as Ru adatoms and nanoparticles diffuse and reach the interface where they aggregate. Nanoparticle growth by aggregation is reduced due to the larger average distance between the nanoparticles. As a direct result, growth by direct precursor adsorption is also reduced as fewer nanoparticles reach a diameter that is larger than the critical size. Overall, the area-restricted and blanket surfaces yield Ru nanoparticles with a similar particle size distribution (PSD), which is a result of the same growth mechanism (Figure 4). Particles reach roughly the same size, although the size of the largest nanoparticle is slightly reduced at all cycle numbers.

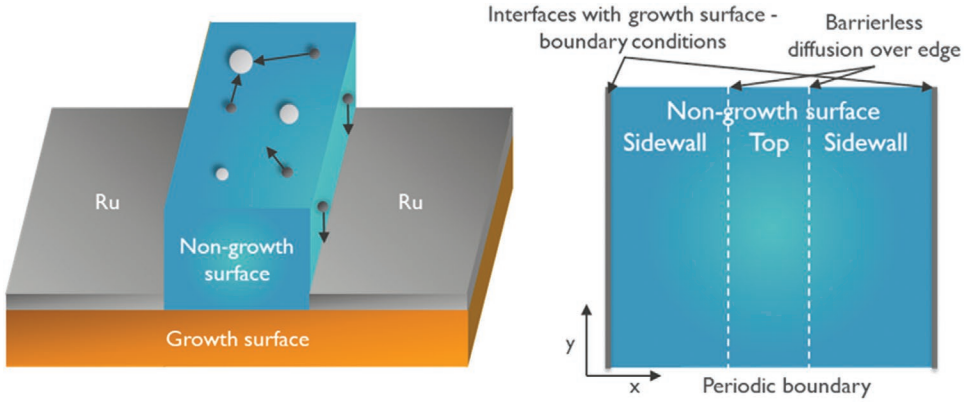

Figure 3. Left: schematic of a 3D line space pattern after ASD. Right: schematic of the planar area-restricted approximation used in the KMC simulations.

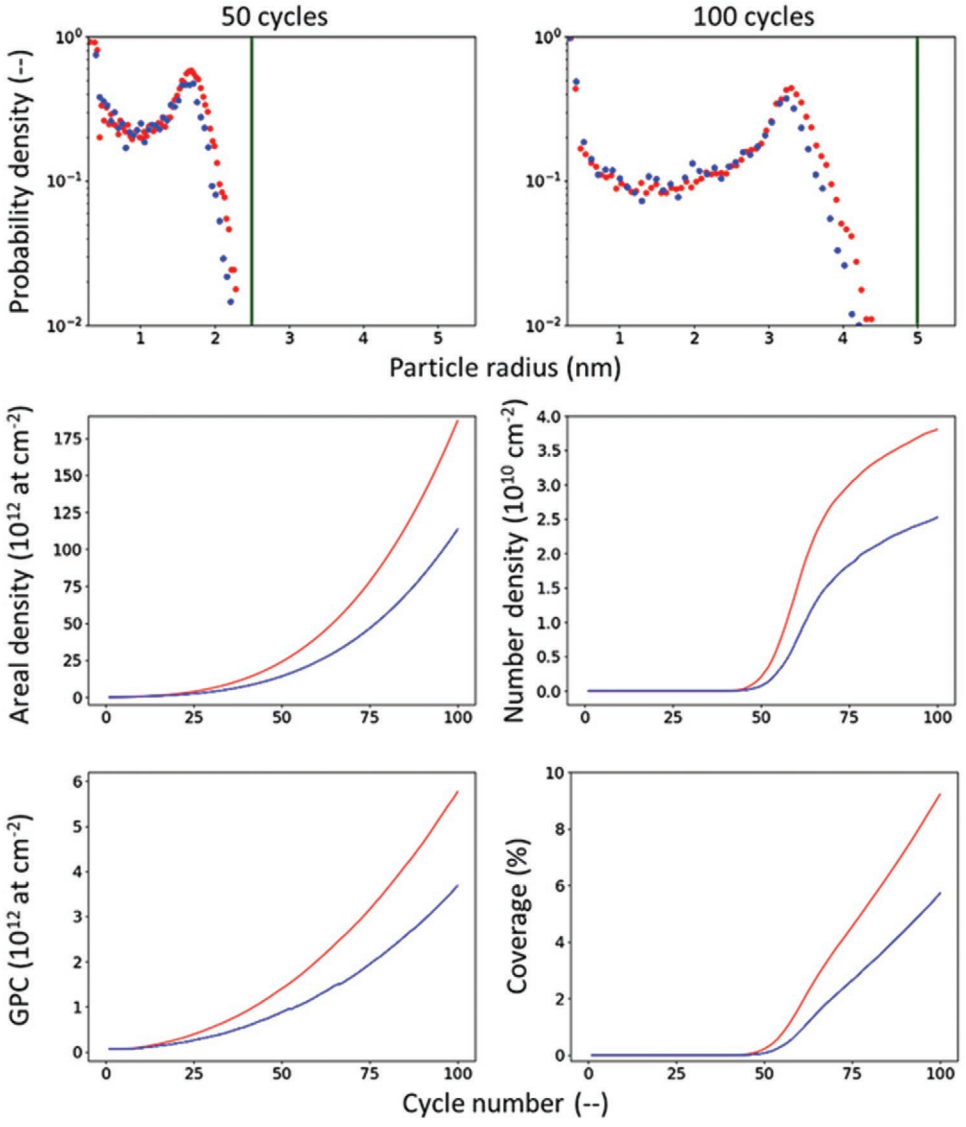

Figure 4. Comparison of Ru ALD growth on a blanket (red) and 200 nm wide area-restricted (blue) SiO_2-$OSi(CH_3)_3$ nongrowth surfaces. Top: probability density of particle radii for a given number of cycles. The green vertical line represents the thickness of an equivalent Ru ALD film on a TiN growth surface. Middle: Ru atom areal density and nanoparticle number density. Bottom: Ru ALD GPC, comprising deposition on both nanoparticles and the free surface, and Ru coverage.

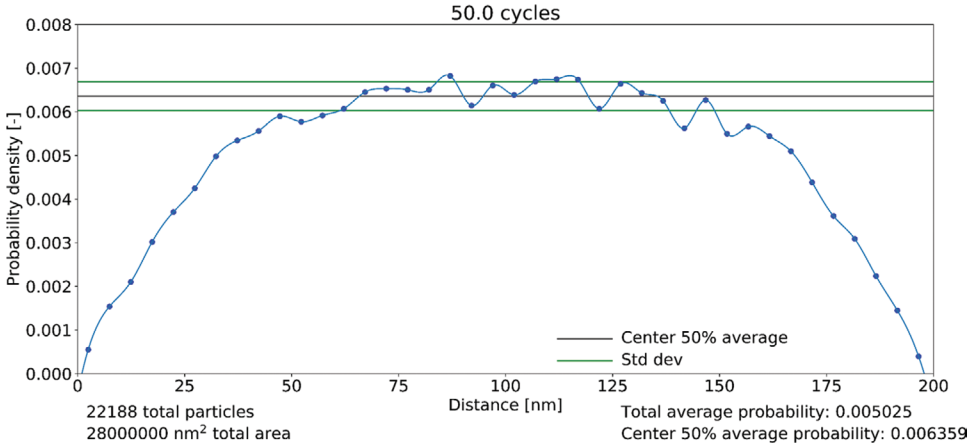

Figure 5. Probability density of finding a Ru nanoparticle at a certain distance along the width of 200 nm wide area-restricted substrate after 50 Ru ALD cycles. The black line marks the average probability of finding a particle in the center 50% of the area-restricted substrate (from 50 to 150 nm), the green lines are the standard deviation. These values serve as a guide to distinguish between the center constant value and the depletion zones closer to the interface. The blue line serves as a guide to the eye.

The diffusion of Ru adatoms and particles does not only impact the overall amount of deposited Ru on the non-growth area, but it also affects the spatial distribution of the Ru adspecies (**Figure 5**). We observe a much lower Ru nanoparticle number density close to the interfaces with the growth area as compared to the center of the nongrowth area. This is due to the average diffusion length of Ru adatoms (18 nm), which is much smaller compared to the line width (200 nm). The Ru atom areal and nanoparticle number densities therefore gradually increase with increasing distance from the interface and reach a steady value at a distance of 50 nm from the interface. Henceforth, we will refer to the zones on the non-growth area less than 50 nm from the interfaces as depletion zones. After 50 ALD cycles, the average nanoparticle number density in the depletion zones is 57% lower compared to the density on blanket substrates, while the Ru atom areal density is 65% lower. In the center of the 200 nm wide area-restricted substrate, at a distance of more than 50 nm from both interfaces with the growth area, we find a constant nanoparticle number density. Still, the nanoparticle number density at the center is 9% lower compared to blanket substrates, while the Ru atom areal density is 18% lower.

The width of the depletion zone (50 nm) is mainly determined by the likelihood of an adatom encountering another adatom, which decreases as the distance to the growth interface decreases. For this reason, fewer large, immobile particles are formed in the depletion zone, which in turn prevents the fast growth by direct precursor adsorption. This self-reinforcing mechanism based on the size-dependent reactivity of the Ru nanoparticles contributes to a depletion zone extending 50 nm from the interface with the growth substrate, i.e., almost three times the average diffusion length (18 nm).

The depletion has a limited impact on the particle size distributions, as most of the particles are located in the center of the area-restricted substrate. As a result, the PSD is similar for Ru ALD on the area-restricted and blanket substrates. The average particle radius is only slightly smaller for 200 nm wide area-restricted substrates compared to blanket substrates as shown by the PSD (Figure 4, top). On the other hand, we find that the size of the largest nanoparticle is slightly reduced at all cycle numbers. This indicates that the same mechanism that leads to depletion extends throughout the 200 nm wide line: diffusion to and collection at the growth interface reduces the nanoparticle number density of nanoparticles over the entire area-restricted substrate. This reduces the likelihood of nanoparticle growth by aggregation, limits the size of the nanoparticles and as such their reactivity toward precursor adsorption by the catalytic effect.

To experimentally verify the existence of depletion zones in nanopatterns, 42 cycles of Ru ALD were applied on SiO_2/TiN line-space patterns with a 90 nm repeating unit (pitch) (see Experimental section). The patterns were treated with DMA-TMS before ALD, to obtain a SiO_2-$OSi(CH_3)_3$ non-growth surface while TiN remains reactive.[32,39] The spatial distribution of Ru nanoparticles on the SiO_2 sidewalls was studied by scanning-tunneling electron microscopy (STEM). Particle size distributions and coverages are extracted from the images for three equally-sized bands on the sidewall (**Figure 6**).

The STEM results confirm that diffusion in Ru AS-ALD creates a depletion zone with lower Ru nanoparticle coverage near the interface with the growth surface, as predicted. The band near the interface with the growth area shows a shift of the particle size distribution to smaller sizes than further away from the interface. The shifted particle size distribution near the interface shows both a smaller average particle size and a 0.7 nm smaller largest particle, when compared to the other bands. This finding corresponds well with the theoretical prediction of reduced defectivity on area-restricted substrates close to the interface. Depletion toward the interface with the TiN growth area is clearly visible in the Ru coverage. As predicted, diffusion results in fewer and smaller particles near the interface. The extent of the depletion is smaller than in the simulations, which predicted a 65% decrease in the total amount of Ru in the depletion zone. This difference could be due to the patterning processes, which expose the sidewall to CF_4/CHF_3 etchants and an O_2 plasma strip. These treatments could modify surface chemistry and morphology. The role of the top surface and the 3D topography are also not captured in the simulations.

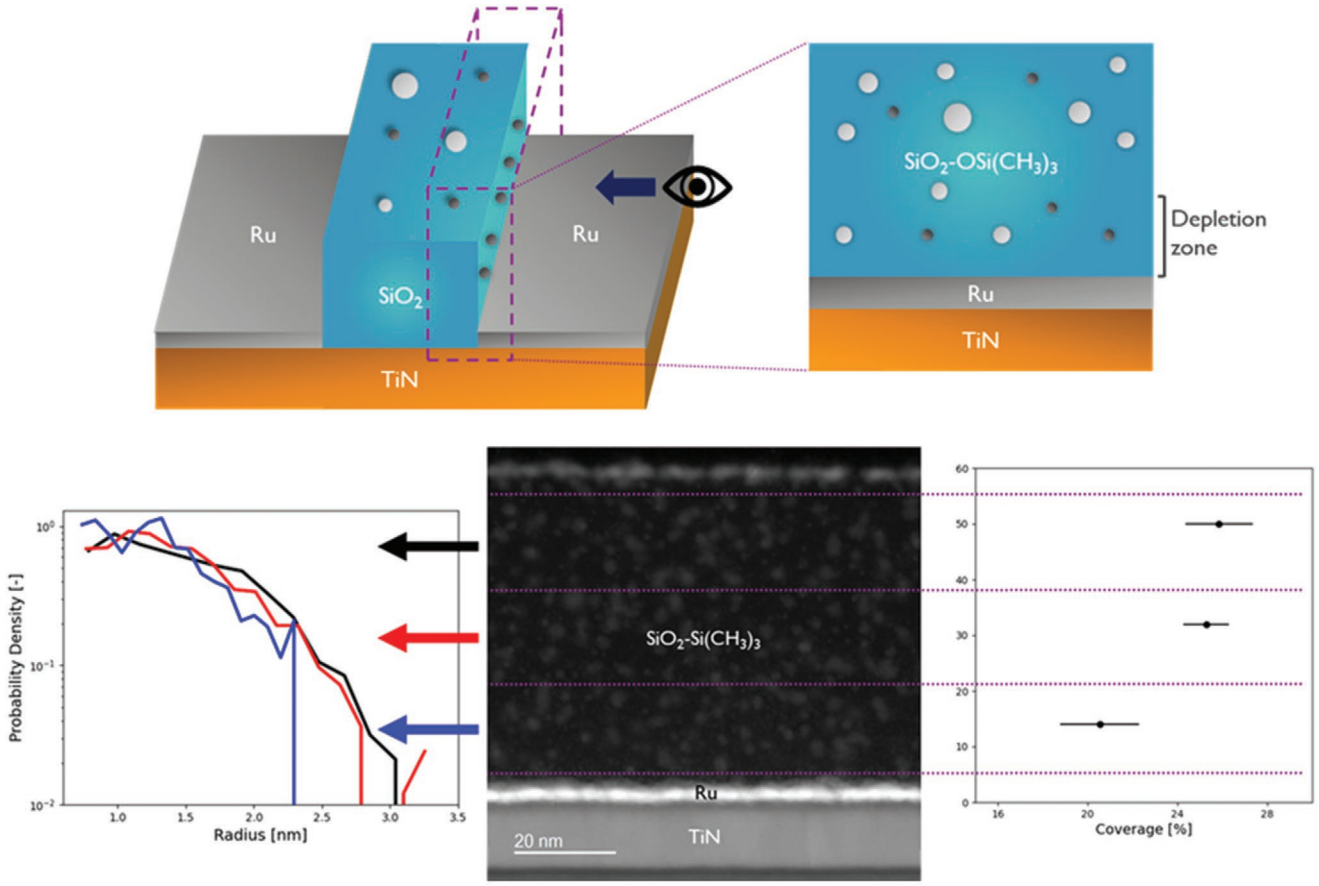

Figure 6. Top: schematic showing the outline of the line-space pattern. Dark blue dashed lines mark the cut of the STEM lamella as prepared by the focused ion beam (FIB). The eye symbol marks the imaging direction perpendicular to the line. A schematic of the resulting view from the STEM imaging direction perpendicular to the lamella is also provided. Bottom center: STEM image of a sidewall after 42 Ru ALD cycles with Ru nanoparticles on the SiO_2-$OSi(CH_3)_3$ non-growth area and a closed Ru film of 2.2 nm thick on the TiN growth area. Bottom left: particle size distribution for three bands on the sidewall (marked by color). Bottom right: Average coverage with standard deviation for three bands on the sidewall.

2.3. Impact of Line Width (20–200 nm) on Ru ASD Growth Mechanism

Reducing the area-restricted substrate width drastically decreases the Ru atom areal density on the nongrowth surface (**Figure 7**). As the two growth interfaces come closer, there is a higher probability of collection of particles at the interface with the growth area. Interestingly, we find a sharp decline in the Ru atom areal density at a line width of 50 nm: reducing the line width from 200 to 50 nm results in a thousand-fold decrease in the Ru atom areal density and in much smaller particles. This thousand-fold decrease in Ru atom areal density is related to a synergetic effect of diffusion and size-dependent reactivity of the Ru nanoparticles during ALD. For line widths of 50 nm and smaller, the Ru nanoparticles are captured at the growth interface before they can aggregate and reach the critical size where growth by precursor adsorption and catalytic reactions start to occur.

Indeed, also the size of the Ru particles dramatically decreases with decreasing area-restricted substrate width for line widths of 50 nm and smaller due to the synergetic effect of diffusion and size-dependent reactivity. To investigate the size of the largest

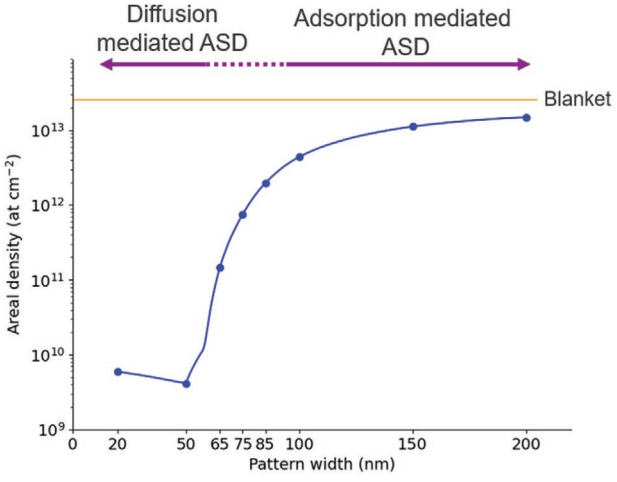

Figure 7. Ru atom areal density after 50 cycles of Ru ALD as a function of area-restricted substrate width. The green line represents the Ru atom areal density on a blanket substrate. The continuous blue line serves as a guide to the eye.

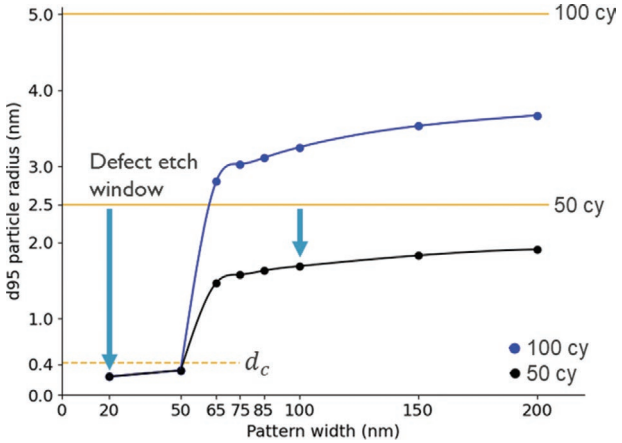

Figure 8. For area-restricted substrate widths below 50 nm, diffusion of Ru adspecies to the growth surface keeps particles smaller than the critical radius, which drastically reduces deposition on the non-growth surface. The 95th percentile Ru particle radius is plotted as a function of area-restricted substrate width for 50 and 100 cycles Ru ALD. The orange lines represent the thickness of an equivalent Ru film on TiN, a typical growth surface. The critical radius is marked by a dashed line. The defect etch is illustrated for 20 and 100 nm wide area-restricted substrates after 50 cycles. The continuous blue and black lines serve as guides to the eye.

particles, we collect the 95th percentile particle radii, as using the 95th percentile will reduce the impact of outliers (**Figure 8**). Even for 100 ALD cycles, 95% of the particles stay smaller than 0.3 nm in radius. This means that these particles do not grow by adsorption, as the minimum radius needed for catalytic activity is 0.43 nm (Figure 8). Interestingly, the size of these particles does not increase as a function of the number of ALD cycles for up to at least 1000 cycles (which would correspond to 50 nm Ru on a blanket TiN surface). This confirms that Ru nanoparticles are effectively captured at the interface with the growth area before their growth by means of adsorption is catalyzed, and the defect capture mechanism persists even during extensive ALD cycles.

Despite the drastic impact of diffusion in the non-growth area, we expect a limited impact on the steady-state GPC on the growth area. The low adsorption rate of the EBECHRu precursor on the non-growth area (6.3 10^{-4} Ru at nm^{-2} cy^{-1}) in combination with the prevented adsorption of EBECHRu on the Ru nanoparticles due to the lack of the catalytic activity result in a small flux of Ru atoms from the nongrowth to growth area. Previously, the steady-state GPC on the TiN growth area was shown to be much faster at 3.7 Ru at nm^{-2} cy^{-1}.[41] We therefore expect that the diffusion processes will not significantly affect the growth rate on the growth area in line patterns. This is confirmed by cross-section TEM of the line-space pattern after ALD (Supporting Information). The cross-section demonstrates that the Ru film thickness is uniform over the growth area, with no measurable thickness increase near the interface with the non-growth surface. This is in contrast to the diffusion-mediated ASD by (carbonyl)(cyclohexadienyl)Ru/H_2 CVD, where the precursor adsorption rates on the growth and nongrowth areas are similar and the average diffusion length (140 nm) is an order of magnitude larger.[12] In that case, a large flux of Ru adspecies from the nongrowth area to the growth area resulted in enhanced growth rates for ASD versus blanket CVD.[25]

Finally, we discuss the impact on selectivity. The common definition of selectivity is given in Equation 3:[27]

$$s = \frac{\theta_G - \theta_{NG}}{\theta_G + \theta_{NG}} \tag{3}$$

With s the selectivity, θ_G the Ru atom areal density on the growth area and θ_{NG} the Ru atom areal density on the non-growth area. Only a qualitative prediction of enhanced selectivity can be made as the deposition on TiN was not studied by the same methods as deposition on SiO_2-$OSi(CH_3)_3$. Ru ALD on a TiN growth surface occurs fast with a steady-state GPC of 0.05 nm cy^{-1} and is known to be independent of growth area dimensions of at least 36 nm and larger.[38,41] We consider that the Ru atom areal density (θ_G) on the TiN growth surface does not depend on the growth area line width, and the more-than-linear dependence of the Ru atom areal density (θ_{NG}) on the SiO_2-$OSi(CH_3)_3$ nongrowth surface width. Together, these two dependencies will result in a selectivity increase with decreasing dimensions of the area-restricted nongrowth area. However, this prediction relies on the assumption of no pattern dependence of deposition on the growth area.

2.4. ASD Growth Regimes and Defect Mitigation

Our findings predict two ASD growth regimes for Ru ASD by ALD, depending on the line width (Figure 7). For a line width of the nongrowth area of 65 nm and larger, ASD is dominated by the differences in the adsorption kinetics on the growth and nongrowth surface area. In this regime, additional passivation and/or defect mitigation are necessary as Ru nanoparticles grow in the non-growth area, as demonstrated here and previously.[33,38] The maximum size of the particles and how it compares to the Ru film thickness on the growth area is important when assessing isotropic, nonselective defect etching as defect mitigation approach. A defect-free ASD condition can be obtained if all particles, including the largest ones, are fully etched, while a closed ASD-grown film remains on the growth area. A simplified metric to predict the ASD defect etch window is the difference between the Ru film thickness and the maximum island height, assuming that films and particles are etched at the same rate. The maximum island height is indicated by the 95th percentile particle radius (Figure 8 For a 200 nm wide area-restricted substrate, the defect etch window is similar to that for blanket substrates, i.e., 1.3 nm after 100 cycles. Cycles of passivation/ALD/etch can be used to extend the Ru thickness while maintaining good selectivity.

An even more positive perspective is provided for Ru ALD when the line widths of the nongrowth area are 50 nm and smaller. In this case, the ASD is governed by adsorption as well as diffusion and nanoparticle growth is inhibited by the size-dependent reactivity. Defectivity is largely suppressed by diffusion to the growth area and any remaining Ru nanoparticles are so small that they are not susceptible to precursor adsorption. As these particles remain smaller than the critical diameter of 0.85 nm even for extensive ALD cycles, a single corrective etch after passivation and ALD can be effective. The calculations therefore predict that a high selectivity (see ref. [3,27]) can

be maintained for much higher Ru thicknesses, up to at least 50 nm. While for adsorption-based ASD with a line width of 200 nm, the defect etch window is small after 100 ALD cycles (corresponding to 5 nm Ru on the growth surface), the window widens to 4.7 nm for diffusion mediated ASD with a line width of 20 nm. This diffusion-mediated ASD regime provides us with a positive outlook for the removal of the minor amount of Ru defects by brief etching.

3. Conclusion

Our combined theoretical-experimental study of Ru ASD by ALD reveals a synergetic effect of surface diffusion and size-dependent reactivity of Ru nanoparticles in nanoscale patterns with dimensions ≤ 50 nm. This mechanism limits defectivity during Ru ASD, as Ru nanoparticles are effectively captured at the growth surface interface before growth by adsorption is catalyzed. Ru nanoparticles that exist in very low concentrations on the nongrowth surface area are so small that effective removal by a one-step nonselective, isotropic defect etch process should be straightforward. Our predictions of low defectivity at small pattern sizes show great promise for application in nanoelectronic device fabrication. However, our work also illustrates the need for studies of ASD mechanisms in nanoscale patterns with small dimensions, as different phenomena may occur due to the close proximity of the growth and nongrowth surface. Surface and/or gas phase diffusion during ASD by ALD and CVD in nanoscale patterns merits further investigation. The KMC simulations were found to be a valuable tool in that respect. Still, the predictive ability of the KMC simulations could be further improved by considering growth as well as nongrowth area, topography, and surface modifications inherent to patterning. It would also be interesting to investigate whether diffusion in nanopatterns might be enhanced by tuning coreagent exposure and substrate temperature.

4. Experimental Section

Ru ASD is achieved by selectively passivating the SiO_2 nongrowth surface with DMA-TMS. The DMA-TMS treatment renders the surface methyl-terminated.[47] The EBECHRu/O_2 island-like ALD growth rate will then be reduced significantly due to inhibited precursor adsorption.[32,39] The DMA-TMS does not react extensively with metal and metal nitride substrates, such as TiN, and does not noticeably reduce the growth rate of EBECHRu/O_2 ALD on TiN (0.05 nm cy^{-1}). In a pattern defined by a SiO_2 nongrowth surface area and a TiN growth surface area, ASD of Ru metal on metal nitride is then enabled.[38,40]

Experimental growth curves on blanket substrates were performed on 300 mm Si[100] wafers. 75 nm hydrophilic SiO_2 (2.5 —OH groups per nm^2) was grown by plasma-enhanced ALD in an ASM Eagle 12 reactor at 75 °C. The DMA-TMS treatment was performed by static exposure in a TEL Tactras system with shower head-type reactor. The wafers were kept at 5 Torr N_2 at 250 °C for 10 min to ensure clean surfaces. The N_2 was then evacuated and subsequently replaced by 500 sccm DMA-TMS and 350 sccm N_2 to a total pressure of 5 Torr. The wafers were exposed to this ambient for 5 min each. EBECHRu/O_2 ALD was performed in an ASM Pulsar 3000 reactor on a Polygon8300 platform.[41] An ALD cycle consisted of 5 s EBECHRu, 5 s N_2, 0.4 s O_2, 3 s N_2. The ALD process was shown to be self-limiting on TiN and SiO_2.[41] Note that the self-limiting character on SiO_2-$OSi(CH_3)_3$ was not investigated. As such, the extent of growth inhibition and nanoparticle growth could depend on the precursor dose and on the total cycle time.

Line-space patterns with 45 nm critical dimension were created on 300 mm Si[100] wafers by physical vapor deposition (PVD) of 15 nm TiN in an AMAT Endura tool. On top of the TiN, 75 nm plasma-enhanced ALD SiO_2 was grown in an ASM Eagle 12 reactor at 75 °C. The lithography stack on SiO_2 was composed of 100 nm spin-on-carbon (SOC), 30 nm spin-on-glass (SOG), 29 nm antireflective coating and 105 nm photoresist, which was exposed in a 193 nm immersion ASML Twinscan NXT:1950i. The pattern was transferred into the SiO_2 layer until exposure of the TiN layer by CF_4/CHF_3 etch, followed by an O_2 plasma strip in a TEL Tactras tool. Finally, the patterns were cleaned to remove possible F contamination. DMA-TMS and ALD processing were identical to those discussed above.

The Ru atom areal density after 1 ALD cycle was determined by TXRF in a Rigaku TXRF300 tool with a 24 keV beam. Ru atom areal density for other cycles was determined by Rutherford backscattering spectrometry (RBS) with a 1.523 MeV He^+-ion beam. Samples were imaged by SEM in a FEI Helios 460 microscope or by STEM in a FEI Tecnai F30 ST microscope. PSDs and nanoparticle number densities were measured on the obtained images in ImageJ by extracting particle areas and converting those to radii by assuming circular particle shapes. Surface roughness was determined by AFM with a Bruker Dimension Icon PT tool.

Supporting Information

Supporting Information is available from the Wiley Online Library or from the author.

Acknowledgements

J.J.C. is SB PhD fellow at FWO (1SB4319N).

Conflict of Interest

The authors declare no conflict of interest.

Data Availability Statement

The data that support the findings of this study are available from the corresponding author upon reasonable request.

Keywords

area-selective deposition, atomic layer deposition, diffusion, nanoelectronics, ruthenium

Received: May 26, 2021
Revised: August 11, 2021
Published online:

[1] M. M. Waldrop, *Nature* **2016**, *530*, 144.
[2] A. J. M. Mackus, A. A. Bol, W. M. M. Kessels, *Nanoscale* **2014**, *6*, 10941.
[3] A. J. M. Mackus, M. J. M. Merkx, W. M. M. Kessels, *Chem. Mater.* **2019**, *31*, 2.
[4] R. Clark, K. Tapily, K. H. Yu, T. Hakamata, S. Consiglio, D. O'Meara, C. Wajda, J. Smith, G. Leusink, *APL Mater.* **2018**, *6*, 058203-058203-12.

[5] H. S. Suh, A. Delabie, S. Armini, *Semiconductor Digest* **2020**, *2*, 14.
[6] J. O. Carlsson, *Crit. Rev. Solid State Mater. Sci.* **1990**, *16*, 161.
[7] M. R. Goulding, *J. Phys. IV* **1991**, *1*, 745.
[8] U. Jansson, J. O. Carlsson, *J. Vac. Sci. Technol., A* **1988**, *6*, 1733.
[9] J. T. Fitch, *J. Electrochem. Soc.* **1994**, *141*, 1046.
[10] F. Grillo, TU Delft, Delft **2018**, http://pure.tudelft.nl/ws/portalfiles/portal/44997010/Thesis_Final_FG.pdf (accessed: August 2021).
[11] F. Grillo, J. A. Moulijn, M. T. Kreutzer, J. R. van Ommen, *Catal. Today* **2018**, *316*, 51.
[12] F. Grillo, J. Soethoudt, E. A. Marques, L. de Martin, K. Van Dongen, J. R. Van Ommen, A. Delabie, *Chem. Mater.* **2020**, *32*, 9560.
[13] J. Soethoudt, F. Grillo, E. A. Marques, J. R. van Ommen, Y. Tomczak, L. Nyns, S. Van Elshocht, A. Delabie, *Adv. Mater. Interfaces* **2018**, *5*, 1800870.
[14] N. E. Richey, C. de Paula, S. F. Bent, *J. Chem. Phys.* **2020**, *152*, 040902.
[15] J. Dendooven, S. P. Sree, K. De Keyser, D. Deduytsche, J. A. Martens, K. F. Ludwig, C. Detavernier, *J. Phys. Chem. C* **2011**, *115*, 6605.
[16] W. L. Gladfelter, *Chem. Mater.* **1993**, *5*, 1372.
[17] B. Korgel, R. F. Hicks, *J. Cryst. Growth* **1995**, *151*, 204.
[18] Z. Zhang, M. G. Lagally, *Science* **1997**, *276*, 377.
[19] S. M. Gates, *Chem. Rev.* **1996**, *96*, 1519.
[20] J. O. Carlsson, *Vacuum* **1990**, *41*, 1077.
[21] M. Bartek, P. T. J. Gennissen, P. J. French, R. F. Wolffenbuttel, *presented at The 8th International Solid-State Sensors and Actuators Conference*, Stockholm, Sweden **1995**.
[22] X. Wang, J. Hartmann, M. Mandl, M. Sadat Mohajerani, H.-H. Wehmann, M. Strassburg, A. Waag, *J. Appl. Phys.* **2014**, *115*, 163104.
[23] S. Jiang, C. Merckling, W. Guo, N. Waldron, M. Caymax, W. Vandervorst, M. Seefeldt, M. Heyns, *J. Cryst. Growth* **2014**, *391*, 59.
[24] B. D. Joyce, J. A. Baldrey, *Nature* **1962**, *195*, 485.
[25] A. Delabie, AVS ALD/ALE 2020 Tutorial **2020**, 42, https://www.pathlms.com/avstechnicallibrary/events/2008 (accessed: August 2021).
[26] P. Klement, D. Anders, L. Gümbel, M. Bastianello, F. Michel, J. R. Schörmann, M. T. Elm, C. Heiliger, S. Chatterjee, *ACS Appl. Mater. Interfaces* **2021**, *13*, 19398.
[27] G. N. Parsons, R. D. Clark, *Chem. Mater.* **2020**, *32*, 4920.
[28] F. Grillo, H. V. Bui, J. A. Moulijn, M. T. Kreutzer, J. R. van Ommen, *J. Phys. Chem. Lett.* **2017**, *8*, 975.
[29] A. J. M. Mackus, M. J. Weber, N. F. W. Thissen, D. Garcia-Alonso, R. H. J. Vervuurt, S. Assali, A. A. Bol, M. A. Verheijen, W. M. M. Kessels, *Nanotechnology* **2016**, *27*, 034001.
[30] J. Dendooven, R. K. Ramachanan, E. Solano, M. Kurttepeli, L. Geerts, G. Heremans, J. Ronge, M. M. Minjauw, T. Dobbelaere, K. Devloo-Casier, J. A. Martens, A. Vantomme, S. Bals, G. Portale, A. Coati, C. Detavernier, *Nat. Commun.* **2017**, *8*, 1074.
[31] F. Grillo, H. Van Bui, D. La Zara, A. A. I. Aarnink, A. Y. Kovalgin, P. Kooyman, M. T. Kreutzer, J. R. van Ommen, *Small* **2018**, *14*, 1800765.
[32] J. Soethoudt, Y. Tomczak, B. Meynaerts, B. T. Chan, A. Delabie, *J. Phys. Chem. C* **2020**, *124*, 7163.
[33] M. F. J. Vos, S. N. Chopra, M. A. Verheijen, J. G. Ekerdt, S. Agarwal, W. M. M. Kessels, A. J. M. Mackus, *Chem. Mater.* **2019**, *31*, 3878.
[34] R. Vallat, R. Gassilloud, B. Eychenne, C. Vallee, *J. Vac. Sc. Technol., A* **2017**, *35*, 01B104.
[35] S. K. Song, H. Saare, G. N. Parsons, *Chem. Mater.* **2019**, *31*, 4793.
[36] S. M. George, Y. Lee, *ACS Nano* **2016**, *10*, 4889.
[37] H. Saare, S. K. Song, J. Kim, G. N. Parsons, *J. Appl. Phys.* **2020**, *128*, 105302.
[38] J. Soethoudt, H. Hody, V. Spampinato, A. Franquet, B. Briggs, B. T. Chan, A. Delabie, *Adv. Mater. Interfaces* **2019**, *6*, 1900896.
[39] J. Soethoudt, S. Crahaij, T. Conard, A. Delabie, *J. Mater. Chem. C* **2019**, *7*, 11911.
[40] R. Khan, B. Shong, B. G. Ko, J. K. Lee, H. Lee, J. Y. Park, I. K. Oh, S. S. Raya, H. M. Hong, K. B. Chung, E. J. Luber, Y. S. Kim, C. H. Lee, W. H. Kim, H. B. R. Lee, *Chem. Mater.* **2018**, *30*, 7603.
[41] M. Popovici, B. Groven, K. Marcoen, Q. M. Phung, S. Dutta, J. Swerts, J. Meersschaut, J. A. van den Berg, A. Franquet, A. Moussa, K. Vanstreels, P. Lagrain, H. Bender, M. Jurczak, S. Van Elshocht, A. Delabie, C. Adelmann, *Chem. Mater.* **2017**, *29*, 4654.
[42] C. Ratsch, A. Zangwill, P. Milauer, D. D. Vvedensky, *Phys. Rev. Lett.* **1994**, *72*, 3194.
[43] C. Ratsch, J. A. Venables, *J. Vac. Sci. Technol., A* **2003**, *21*, S96.
[44] E. S. Dana, *A Text-Book of Mineralogy*, (Ed: W. E. Ford), John Wiley & Sons, New York **1922**, pp 94–98.
[45] R. Van Hardeveld, F. Hartog, *Surf. Sci.* **1969**, *15*, 189.
[46] J. Hämäläinen, M. Ritala, M. Leskelä, *Chem. Mater* **2014**, *26*, 786.
[47] J. J. Fripiat, J. Uytterhoeven, U. Schobinger, H. Deuel, *Helv. Chim. Acta* **1960**, *23*, 7.